American Journal of Data Science and Artificial Intelligence (AJDSAI)

ISSN: 3069-3632 (ONLINE)

VOLUME 2 ISSUE 1 (2026)

PUBLISHED BY
E-PALLI PUBLISHERS, DELAWARE, USA

American Journal of Data Science and Artificial Intelligence (AJDSAI)

Volume 2 Issue 1, Year 2026
ISSN: 3069-3632 (Online)
DOI: https://doi.org/10.54536/ajdsai.v2i1.5278
https://journals.e-palli.com/home/index.php/ajdsai

Thermal Fault Analysis and Optimisation of Induction Motors Using Current and Temperature Signals with Artificial Intelligence

Daniel Kumi Owusu[1*], Christian Kwaku Amuzuvi[2], Joseph Cudjoe Attachie[3]

Article Information

Received: June 20, 2025

Accepted: December 12, 2025

Published: March 08, 2026

Keywords

Autoencoder, Current-Temperature Signals, Induction Motors, Predictive Maintenance, Thermal Fault Detection

ABSTRACT

Induction motors are widely used in industry, yet thermal stresses caused by electrical and mechanical losses reduce their reliability, efficiency, and service life. This study presents an autoencoder-based, non-intrusive fault-detection framework that utilises synchronised current and bearing-housing temperature signals. Data quality measures, min-max normalisation, and sliding-window segmentation support robust time-series learning of normal operating patterns. Implemented in TensorFlow/Keras and trained over 12 epochs using the Adam optimizer with L2 regularisation, the model achieved stable convergence by the sixth epoch, with training loss at 0.0345 MSE and validation loss at 0.0265 MSE. Anomalies were detected through reconstruction errors, applying a 97th percentile threshold of 3.5288 to distinguish normal behaviour from fault conditions. Performance metrics demonstrate strong diagnostic ability, including a True Positive Rate of 94.5%, False Positive Rate of 4.3%, Precision of 95.1%, Recall of 94.5%, and an F1-score of 94.8%. The results confirm reliable detection of current and temperature deviations, enabling early fault intervention, reducing unplanned downtime, and improving energy efficiency. The approach generalises well across various operating conditions and offers a scalable foundation for intelligent condition monitoring of industrial motor fleets.

INTRODUCTION

Induction motors underpin modern industrial frameworks by driving an extensive range of mechanical functions, thanks to their cost-effectiveness, reliability, and ease of operation (Usman & Saxena, 2025). Even with their robust construction and widespread deployment, diverse thermal challenges markedly undermine their service duration and functional dependability. Insight into thermal characteristics remains crucial for induction motors to achieve maximum efficiency and sidestep disastrous malfunctions (Aires *et al.*, 2025). Various mechanisms in induction motors produce heat, collectively intensifying the system's thermal burden. Electrical losses represent the principal origin, encompassing copper losses in stator and rotor windings arising from current passage, iron losses in the magnetic core due to hysteresis and eddy currents, plus extraneous losses from harmonics and supply imbalances (Azab, 2025).

Mechanical losses further contribute to heat buildup via bearing friction, windage from rotor motion, and excess thermal and mechanical strain caused by misalignment (Paul & Manohar, 2025). External factors frequently intensify thermal challenges during induction motor operation. Overloaded conditions compel motors to draw surplus current, resulting in exponential rises in copper losses and consequent temperature escalation. Inadequate cooling mechanisms fail to sustain thermal balance under standard loads, while elevated ambient temperatures hinder effective heat dissipation (Tikadar *et al.*, 2024). Suboptimal maintenance practices introduce further thermal stressors, including clogged cooling passages, degraded bearings, and compromised insulation, all of which impair motor functionality. Induction motor thermal breakdowns carry profound economic ramifications, primarily through abrupt failures that trigger unplanned outages, production shortfalls, and substantial replacement expenditures. Progressive thermal harm manifests as winding deterioration, with excessive heat accelerating copper conductor ageing and diminishing electrical conductivity (Abdulkareem, 2025)

Exceeding the temperature limits of insulation materials under thermal overload triggers degradation, culminating in short circuits, ground faults, and potential immediate motor shutdown. Elevated temperatures, along with lubrication deficiencies, activate thermal expansion, accelerating bearing wear and advancing mechanical imbalance and sudden breakdowns (Polo *et al.*, 2025). Thermal strain further erodes motor efficiency via compromised magnetic properties and heightened electrical resistance, thereby escalating energy demands and operational expenses (Zeybek *et al.*, 2025).

Nonlinear, complex couplings between thermal dynamics and induction motor performance variables complicate fault diagnosis and remediation, even amid progress in design and safeguarding technologies. Traditional approaches like temperature sensors and thermal overload relays typically activate post-damage, furnishing minimal understanding of underlying thermal profiles (Habyarimana & Adebiyi, 2025).

Standard thermal protection methods fail to foresee

[1] Department of Electrical and Electronic Engineering, Takoradi Technical University, Takoradi, Ghana
[2] Department of Renewable Energy Engineering, University of Mines and Technology, Tarkwa, Ghana
[3] Department of Electrical and Electronic Engineering, University of Mines and Technology, Tarkwa, Ghana
[*] Corresponding author's e-mail: daniel.owusu@ttu.edu.gh

escalating thermal anomalies prior to their evolution into severe disruptions, incurring unexpected halts and substantial monetary setbacks. Contemporary thermal surveillance mechanisms suffer from essential deficiencies that obstruct proactive fault aversion. Predominant emphasis on superficial temperature readings overlooks the subsurface thermal processes fueling fault progression, while deficient predictive frameworks curtail foresight into thermal stress accumulation; concurrently, absent real-time analytical prowess delays intervention (Bahgat *et al.*, 2024). Inadequate differentiation between routine thermal fluctuations and emergent failure precursors is another way older systems cause incorrect alerts or failures to go unnoticed (Venugopal *et al.*, 2023).

Deploying artificial intelligence approaches, notably autoencoders, offers a promising avenue to overcome these constraints via superior anomaly identification and pattern discernment. Yet, a prominent void persists in both academic literature and practical implementations concerning AI-driven thermal anomaly assessment for induction motors. This investigation holds multifaceted relevance for energy stewardship and industrial motor deployments. In terms of reliability, AI-enhanced thermal fault diagnostics heralds a paradigm shift toward prognostic maintenance paradigms capable of forestalling extensive motor collapses. Early thermal anomaly detection and remediation promise substantial cuts in unanticipated stoppages, maintenance expenditures, and motor durability extension. Energy efficiency improvements constitute another pivotal facet of this study's value.

Thermal anomalies often signal declining motor efficiency, thereby increasing energy demands and operational costs. The proposed AI optimisation system identifies and rectifies inefficient conditions, delivering substantial energy reductions in industrial settings. The industrial benefits of this research encompass elevated production output, reduced maintenance requirements, and enhanced process stability. Manufacturing, mining, and water treatment sectors, reliant on motor driven operations, gain considerably from improved thermal defect diagnostics. The study provides a versatile framework for intelligent condition monitoring, extendable to other vital industrial components, thus advancing AI applications in industry. Technologically, it fosters more intricate and reliable surveillance systems through greater insight into AI driven diagnostics.

Combining autoencoders with thermal analysis introduces an innovative strategy, opening pathways for monitoring and optimisation in diverse industrial assets. This investigation centres on applying autoencoder based artificial intelligence for thermal fault detection and optimisation in three phase induction motors. Development, deployment, and validation of AI models form the core, utilising temperature and current data as primary inputs to pinpoint thermal anomalies.

Autoencoder neural networks receive design and training to discern normal thermal patterns and flag deviations indicative of emerging faults. Performance metrics emerge within the scope to affirm the effectiveness of this AI driven methodology.

LITERATURE REVIEW

Mhaske *et al.* (2024) examined elevated temperature effects on electromagnetic behaviour in canned induction motors. Finite Element Method (FEM) analysis via Japan Motor Analysis General-purpose (JMAG) software on a 3.7 kW motor revealed that higher temperatures diminish efficiency and magnetic flux densities. Yu *et al.* (2024) assessed loss distribution influences on temperature profiles in high speed induction motors. Skin effects elevated AC resistance, yet elevated frequencies reduced stator winding losses through fewer conductor turns. Efficient loss distribution methods emerged to curb thermal issues, highlighting amplified stator core losses, rotor cage losses, and wind friction losses at high speeds. Zhao *et al.* (2023) analysed transient startup temperature rises in high voltage, high power density induction motors. A 3D fluid solid coupling model accurately forecasted temperature evolution and distribution across load variations. Elorza *et al.* (2023) assessed electrical and environmental factors influencing Partial Discharge Inception Voltage (PDIV) in motor winding insulation, underscoring temperature's notable role. An analytical model for twisted pairs emerged, alongside evaluation of existing PDIV models up to 180 °C. The researchers proposed that future work should integrate waveform parameters, pulse width, and humidity, while balancing precision and computational efficiency. Soltani *et al.* (2022) analysed temperature fluctuations and copper losses in hairpin windings for Permanent Magnet Synchronous Motors (PMSMs) in racing vehicles. Hairpins offered superior thermal dissipation, lower DC resistance, and elevated fill factors compared to conventional windings. Finite Element Analysis (FEA) and multi-dimensional optimisation revealed substantial efficiency impacts from high temperatures across frequencies.

Tazerart *et al.* (2024) explored strategies to minimise heat losses and enhance current conduction in induction machines for electric vehicle drive systems. Control approaches, such as direct torque control and power factor optimisation, emerged to curb current related losses and elevated efficiency. Flux level management received emphasis as a performance enhancer for machine operation in electric vehicle contexts. Tabora *et al.* (2024) assessed voltage fluctuation impacts on heat production and current distribution in Line Start Permanent Magnet Motors (LSPMM). Undervoltage conditions elevated power factor, reduced temperatures, and improved efficiency to extend motor service life. Voltage optimisation proved essential for curbing heating, given current demands tied to operational and load profiles.

Reyes-Malanche *et al.* (2023) devised a method via current measurement analysis to detect and classify short circuit faults provoking induction motor overheating. Fuzzy

logic combined with phasor scrutiny of phase and line currents pinpointed stator winding faults with high precision. The approach excelled in online monitoring, capturing both incipient and progressed faults. Morikawa and Katsura (2023) examined thermoelectric cooling integration to avert overheating in robot and manipulator motors under high current loads. Thermoelectric cooling outperformed conventional water cooling methods, markedly enhancing motor performance and reliability while permitting extended operation prior to thermal limits. High intermittent power demands in such applications stood to gain substantially.

Morikawa and Katsura (2022) assessed thermoelectric cooling elements to augment heat dissipation in motors for humanoid robots and manipulators. This approach curtailed downtime, forestalled premature failures, and enabled elevated current handling absent overheating. Compact and mobile, the system surpassed traditional water cooling, supporting superior power densities and prolonged runtime.

Al-Quraan *et al.* (2022) examined high current draw in industrial induction motors and found that surplus current accelerated degradation alongside intensified thermal wear on insulation. They devised a control strategy with real-time voltage adjustments according to load conditions, current levels, and ambient temperature, which cut maintenance expenses and boosted energy efficiency by up to 20%.

Zhang *et al.* (2022) developed a technique to calculate power grid short circuit currents, emphasising induction motors' substantial inrush contributions to fault induced overheating. Load conditions and accurate motor models refined short circuit current predictions. Validation occurred through a Central China Power Grid case study.

Bochkarev *et al.* (2021) devised an AC motor heat protection method using phase differences between voltage and current vectors to track stator winding temperature. Anomalies in current vectors triggered timely interventions against overheating. High heat emerged as the primary factor in performance decline and operational interruptions.

MATERIALS AND METHODS

Formulation of an Autoencoder-powered Fault Classification System

Artificial Neural Networks (ANNs) perform well in capturing complicated relationships, managing multivariable dynamics, and facilitating data driven learning. This research harnessed an ANN for induction motor thermal analysis, with current and temperature serving as principal influencers. Accurate prediction of thermal profiles and anomaly identification resulted from this approach. Systematic steps detailed in Figure 1

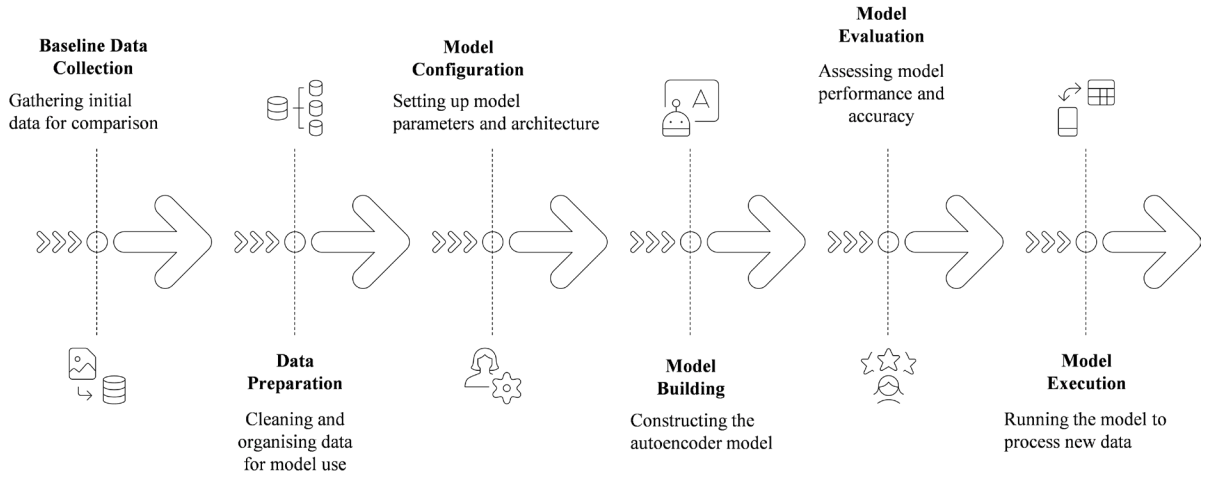

Figure 1: ANN-oriented Autoencoder Framework

guided the ANN model formulation.

Data Quality Enhancement

Current and temperature data were cleaned to remove duplicates, inconsistencies, and inaccuracies, thereby ensuring reliability. Even minor data flaws risked impairing subsequent phases, including optimal machine learning model training and the preservation of data integrity.

Feature Standardisation

Min–max normalisation scaled the input variables to the range of 0 to 1, ensuring equal contribution to the learning process. The normalisation formula was derived as follows:

$$X_{scaled} = \frac{X - X_{min}}{X_{max} - X_{min}} \quad (1)$$

where X_{scalcd} represents the new normalised value between 0 and 1, represents the original value of the feature before scaling ,X_{min} represents the minimum value of the feature in the dataset, and X_{max} represents the maximum value of the feature in the dataset.

Time-Series Structuring

To identify temporal dependencies, the data were arranged into successive overlapping sections. Using a sliding window technique, training used historical sequences to identify recurring patterns and trends in time series.

Partitioning Data into Training and Testing Sets

The dataset was split into subgroups for testing and training. The test set included both healthy and faulty states to assess the autoencoder's ability to detect anomalies, whereas the training set consisted solely of normal machine activities, allowing the autoencoder to record typical behaviour.

Autoencoder System Development

TensorFlow and Keras frameworks facilitated the autoencoder implementation. Its architecture comprised specified hidden layers, neuron counts, optimisation methods, loss functions, and activation functions. The autoencoder enabled unsupervised learning through data compression and extraction of high level features for deep model training.

Architectural Framework of the Autoencoder

The autoencoder (AE) architecture in Figure 2, which represents input layer data as X, hidden layer data as Z, and reconstructed output layer data as X', was provided by Berahmand *et al.* (2024). Its fundamental parts were the encoder and decoder. The original data was restored by the decoder after the encoder reduced the dimensional

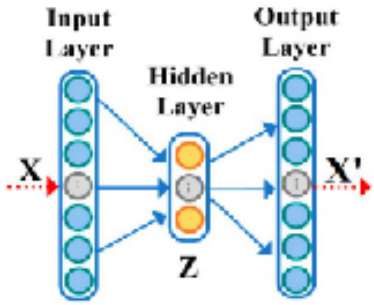

Figure 2: Architecture of the Autoencoder

latent form of the input data.

In the encoding phase, the autoencoder transformed input vector X into code vector Z via encoding function f. Decoding phase then employed function g to revert Z into reconstructed output vector X. Network weights W underwent adjustment to minimise reconstruction error L between original X and its reconstruction, serving as the loss function for parameter tuning. The objective

$$\min_{\theta} J_{AE}(\theta) = \min_{\theta} \sum_{i=1}^{n} L(x_i, z_i) = \min_{\theta} \sum_{i=1}^{n} L(x_i, g_{\theta}(f_{\theta}(x_i))) \quad (2)$$

function of the autoencoder can be expressed as follows: where the number of training data points is represented by n., Z_i is for the ith dimension of the output data, and expresses X_i the training samples at the ith dimension.

The reconstruction error (L) between the input and output data is shown as follows:

$$L(x, z) = \frac{1}{n} \sum_{i=1}^{n} \square X_i - Z_i \square^2 \quad (3)$$

where L (x, z) is the reconstruction error or loss function, x_i is the i^{th} component of the input, z_i is the ith reconstructed value corresponding to x_i, n is the number of features in the input/output vectors, $x_i - z_i$ is the difference between the original input and its reconstruction for the i^{th} element, $(x_i - z_i)^2$ is squared error for the i^{th} element, 1/n is the average of the total squared error ,and is the summation of squared errors across all elements.

The encoder's mapping function can be written as follows:

$$y = f_{\theta}(x) = s(Wx+b) \quad (4)$$

where x is the input vector, W is the weight matrix, b is the bias factor, and s is an activation function.

Furthermore, the decoder's mapping function for the inverse operation is written as follows:

$$z = g_{\theta}(y) = s(W'y+b') \quad (5)$$

where z is the reconstructed version of the original input data, aiming to be as close as possible to the input y, the latent (compressed) representation produced by the encoder is y, and s is specifically chosen as a general activation function, like the sigmoid function or ReLU. W and are weight matrices whilst b and are bias vectors.

Model Training Parameters for the Current and Temperature Autoencoder

The careful selection and modification of training parameters used for the autoencoder model, which used temperature and current data for thermal detection and optimisation to ensure optimal performance, is shown in Table 1.

Table 1: Specifications of the Autoencoder Training Parameters

Parameter Specification	Current and Temperature-Driven Autoencoder
Optimiser	Adam
Initial Learning Rate	0.001
Final Learning Rate	0.0001
Batch Size	64
Regularisation Term (L2)	0.0001
Trained Epochs	12
Best Validation Loss	0.0256
Last Epoch Gradient	0.00035

Training Optimisation Algorithm and Loss Function

To minimise the loss function, the Adam optimiser was used. The computation of reconstruction loss was based on Mean Squared Error (MSE), as illustrated below

$$MSE=\frac{1}{n}\sum_{i=1}^{n}(X_i-\bar{X})^2 \quad (6)$$

where n represents the considered number of data observations or points, $X_{(i)}$ represents the ith data point of the true (original) value, $\sum_{i=1}^{n}$ represents the reconstructed or predicted value of the ith data point by the model,

$(X_i-\bar{X})^2$ is the squared difference between the predicted and actual values, and represents the nth data The mean squared error is obtained by taking the inverse of n, which is the total squared error average, and using the sum of points to determine the overall total squared error.

Autoencoder Model Training Using Current and Temperature Data

The preprocessed temperature and current datasets were used to train the AE. To ensure consistency, the data was normalised using Min-max scaling between 0 and 1 as follows:

$$\text{Min - max scaler} = \frac{x_i - \min(x)}{\max(x) - \min(x)} \quad (7)$$

where max(x) and min(x) are the maximum and minimum values of the feature x, respectively. Using 80% of the data for training, the model was trained across 12 epochs with a batch size of 64.

Training Performance Evaluation

Reconstruction loss (MSE) tracking was used to evaluate the model's performance during training. When validation loss ceased improving for ten (10) consecutive epochs, training was halted to avoid overfitting.

Metrics and Validation Strategy

To evaluate the model's capacity for generalisation, 20% of the dataset was set aside for validation. Mean Squared Error (MSE) was the main evaluation statistic. Furthermore, accuracy and F1 score were calculated to assess classification performance after a threshold was applied to the reconstruction error to separate fault conditions from normal operation.

Testing on Unobserved Data Samples

To verify the resilience of the model, previously unused data covering various induction motor malfunction scenarios were used. It demonstrated dependable fault detection capabilities by successfully identifying anomalies whenever reconstruction errors exceeded a predetermined threshold.

Libraries and Tools for Environment Configuration

The environment was set up using Anaconda and then executed on a GPU-accelerated computer. The implementation was carried out using the following Python libraries:

i. Keras; and
ii. TensorFlow 2.x.

Overview of Code Structure and Workflow

The structure of the codebase was made up of the following modules:

i. data_preprocessing.py: normalisation and reshaping of time-series data;
ii. autoencoder_model.py: description of the encoder, decoder, and complete autoencoder;
iii. train_model.py: early stopping, training loop, and model checkpointing; and
iv. evaluate_model.py: visualisation and analysis of reconstruction error.

Exploratory Data Analysis

Exploratory data analysis was used to find patterns, anomalies, and linkages in the dataset. It also helped find deviations and flaws and acted as a guide for preprocessing and modelling techniques.

RESULTS AND DISCUSSION

Assessment of Current Response Across Different Load Conditions

Temperature data from the motor bearing housings A and B will be subjected to time-series trend analysis to identify unusual thermal patterns. Rolling averages of U, V, and W phase currents under different load conditions will also be investigated to detect electrical instabilities. The rolling average plots of the motor's U, V, and W phase currents under various load scenarios are shown in Figures 3, 4, and 5. Over the course of 40 seconds, the motor phase currents were observed under both faulty and healthy operating situations. The U-phase current, depicted in Figure 3, displays fault features through alternating amplitude rises and falls, particularly initial decreases followed by irregular increases. Such conduct indicates torque demand instability, likely arising from factors such as uneven loading circumstances, mechanical misalignments, or winding breakdown. The healthy waveform, on the other hand, maintains smoother and lower-amplitude changes to show steady torque control and intact electrical insulation. The autoencoder can differentiate between normal and anomalous U-phase current patterns using these time-series features between healthy and faulty states. The V-phase current rolling average plot is shown in Figure 4. The current readings fluctuate irregularly between -0.086 A and -0.084 A under defective conditions, rising slightly above -0.090 A. These anomalies could result from rotor unbalance, varying magnetic field alignment, or partial insulation failure. As a result, the healthy V-phase waveform has

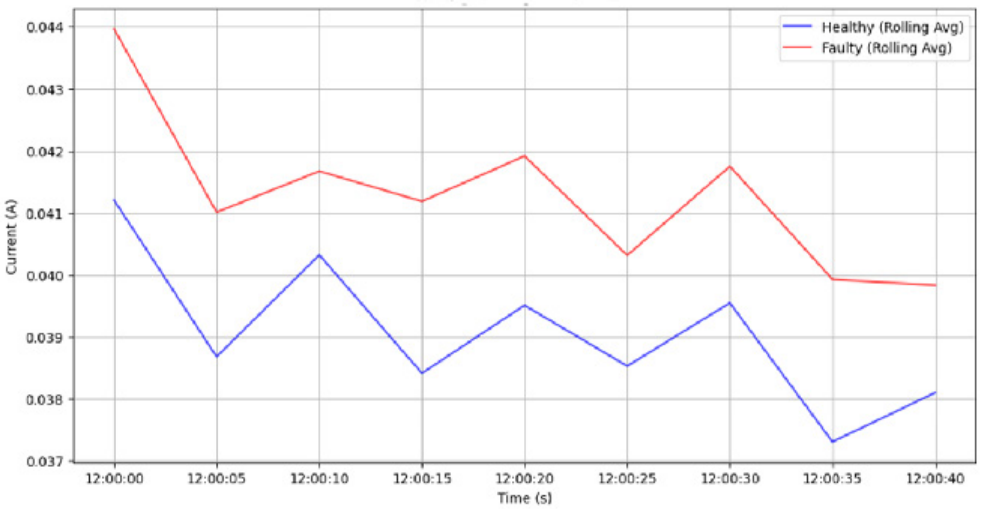

Figure 3: Visualisation of U-phase Current Using Rolling Average

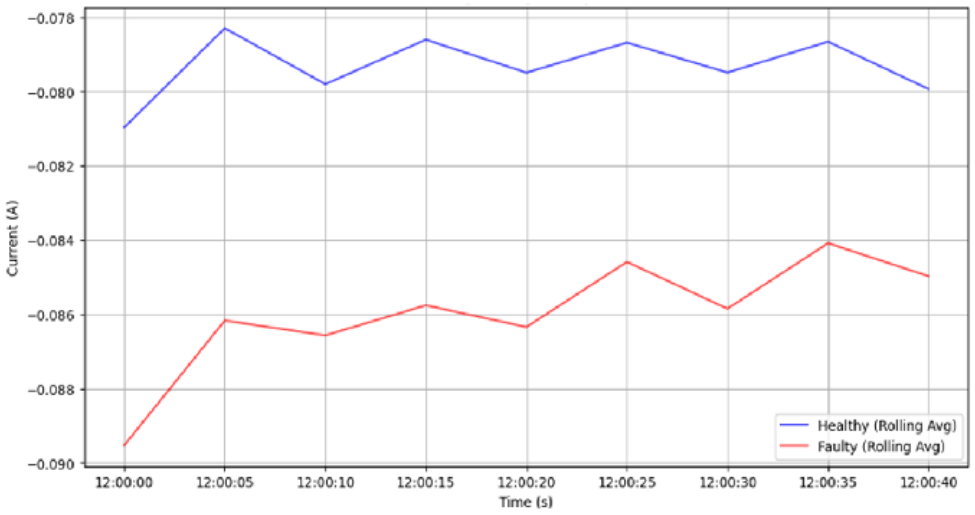

Figure 4: Visualisation of V-phase Current Using Rolling Average

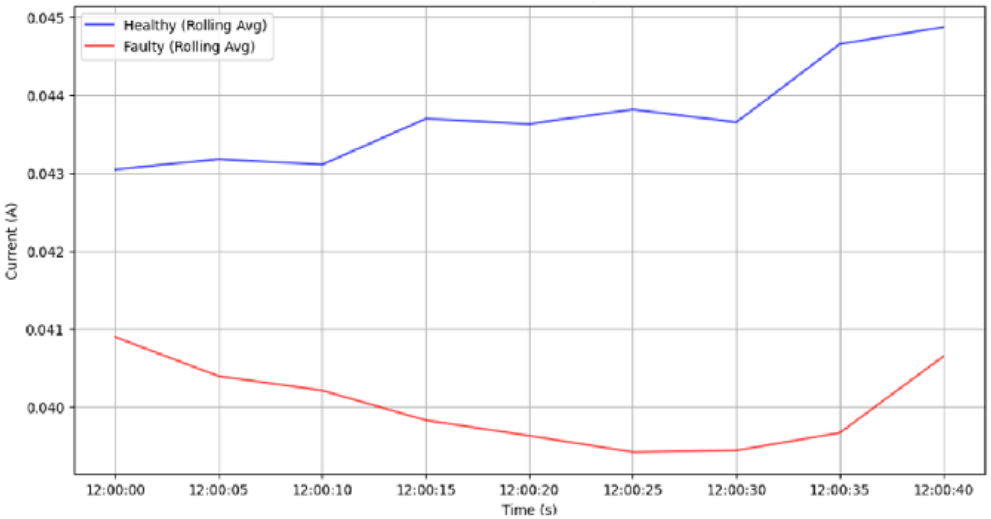

Figure 5: Visualisation of W-phase Current Using Rolling Average

a smoother trend beginning between -0.082 and -0.080 A and stabilising around -0.078 A. Since the averaging window captures elements of the negative half-cycle, the negative values seen on the x-axis represent the properties of alternating current. These trends help the autoencoder model learn the V-phase phase currents' sinusoidal baseline behaviour, which is important for efficient anomaly detection. Under defective conditions, the W-phase current in Figure 5 shows a continuous fall from just around 0.041 A to below 0.040 A, followed by a minor rebound. This suggests an unstable current draw, which is probably brought on by a build-up of electrical resistance or mechanical drag. To depict effective mechanical load balancing and current regulation, the healthy state starts at 0.043 A and gradually increases to almost 0.045 A with little variation.

Examination of Temperature Fluctuation Profiles During Operation

The trend analysis of time-series temperature data from Housings A and B under both healthy and faulty motor conditions is shown in Figures 6 and 7. Housing A showed a higher mean temperature between 30.6°C and 31.5°C under improper operation, with fluctuations occurring within a tighter band of 30.4°C to 30.6°C. The healthy condition, on the other hand, maintained a lower and more consistent range between 25.1°C and 25.7°C. Similarly, compared to lower inferred values under healthy operation, Housing B showed a problematic mean temperature of 29.7°C to 30.5°C, with values fluctuating between 29.4°C and 29.8°C. These increasing temperature trend shifts are indicative of abnormal thermal stress, which may be caused by mechanical misalignments, bearing wear, lubricant deterioration, or increased friction. A closer proximity to the fault cause or increased heat conduction from the affected components are suggested by Housing A's more notable temperature increase. Similarly, Housing B's wider range may point to more thermal instability caused by fluctuations in load, irregularities, or mechanical interactions. These temporal temperature patterns serve as important characteristics for learning baseline thermal behaviour from the perspective of autoencoder modelling. The model can subsequently detect outliers, such as unpredictable fluctuation or

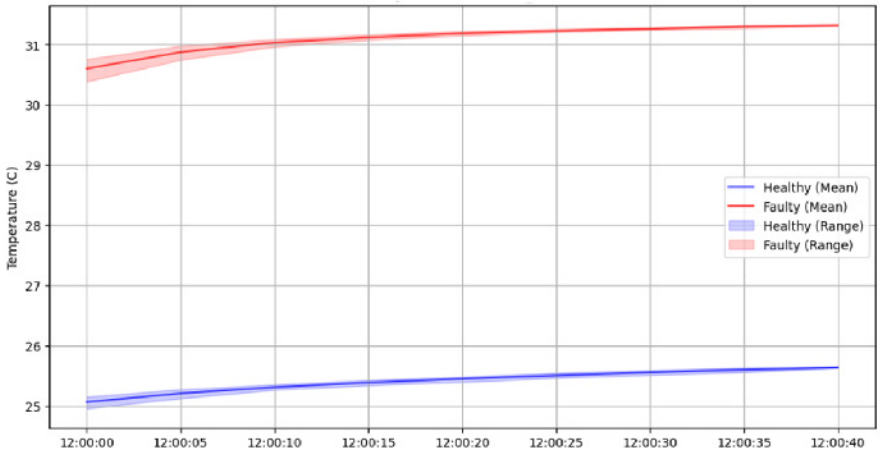

Figure 6: Examination of Temperature Change Dynamics in Motor Housing A

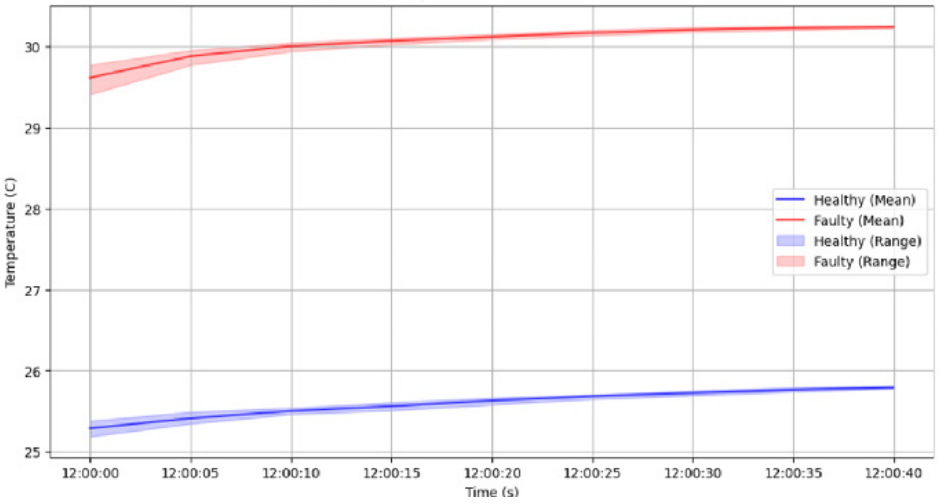

Figure 7: Examination of Temperature Change Dynamics in Motor Housing B

persistent heat elevation, as anomalies through elevated reconstruction errors by capturing these typical operating patterns. Thus, trend analysis enhances the precision and interpretability of unsupervised learning models in predictive maintenance and thermal optimisation of induction motors, in addition to helping with early failure identification.

Correlation Matrix Heatmap for Current and Temperature Signals

The correlation heatmap generated from temperature and current data from the induction motor is shown in Figure 8. The most effective use of correlation heatmaps is for variables that exhibit continuous and linearly connected behaviour over time. Since current and temperature have a direct electromechanical link, they were chosen for this purpose. This is because load variations and resistive heating frequently have an impact on thermal output when motor current varies. These continuous variables are represented by the heatmap's x and y axes, which make it easier to see how they are related. Strong positive correlations between the phase currents and the temperature data from Housings A and B were displayed in the heatmap. Temperature and phase current inputs for anomaly identification were given priority during the model building feature selection procedure based on these findings. The colour gradient of the heatmap ranged from ±1.0. This demonstrates the appropriateness of these signals for correlation analysis in the context of thermal behaviour modelling and analysis and provides visual support for these linkages.

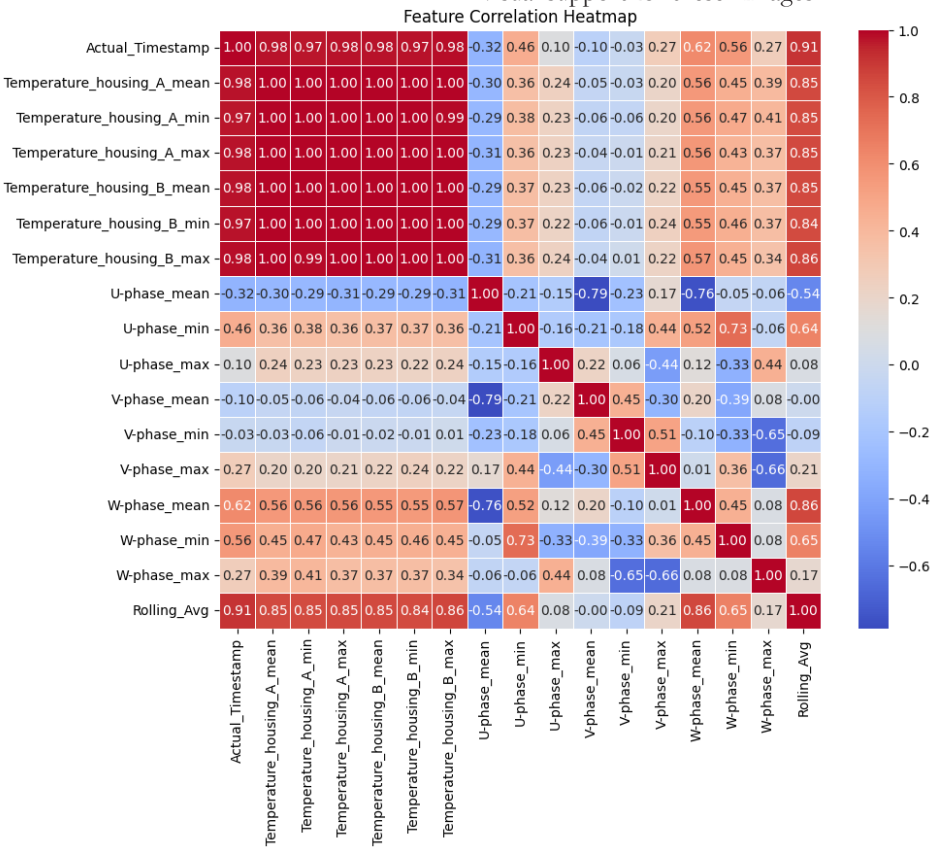

Figure 8: Visual Correlation Map of Motor Current and Temperature Signals.

Learning Curve Analysis of Current and Temperature Responses

The autoencoder learning curve for temperature and current signals is illustrated in Figure 9. The autoencoder model showed robust learning capacity, reducing the training loss from an initial MSE of 0.040. The validation loss followed a similar trajectory, beginning at 0.0385 MSE. Training utilised temperature and current signals. Both training and validation losses converged and stabilised by the sixth (6^{th}) epoch, with training loss slightly higher at roughly 0.0345 MSE, while validation loss settled near 0.0265 MSE. This pattern indicated absence of overfitting and suggested the model had achieved optimal generalisation. The model effectively captured the underlying data structure, preventing the irrelevant fluctuations or reconstruction of noise, as evidenced by minimal loss variance beyond this stage. Subsequently, anomalies related to current and temperature deviations could be reliably identified by means of elevated reconstruction errors contrasting with the learned baseline. These findings affirm the autoencoder's capability as a non-intrusive defect detection mechanism, supporting thermal predictive maintenance and optimisation in induction motor systems.

Detection of Anomalies in Current and Temperature Signals

The distribution of reconstruction errors for current-temperature signals shown in Figure 10 offers valuable

insight into the autoencoder model's capacity to distinguish between normal and abnormal patterns. Most data points exhibit low reconstruction errors, reflecting accurate reconstruction of standard operating conditions. The red dashed line marks the 97th percentile threshold at 3.5288, which functions as the decision boundary for detecting abnormal motor states. Data points exceeding this threshold represent significant deviations from normal operation, indicating possible faults. This threshold effectively segregates typical reconstruction variations from those that suggest anomalous conditions. The distinct separation between the two regions demonstrates that the autoencoder successfully generalised normal current-temperature patterns while failing to reconstruct anomalous ones, which aligns with its intended purpose. These results endorse the model's applicability for real-time monitoring and predictive maintenance in induction motor systems, facilitating early detection of thermal or current-related faults and reducing the likelihood of

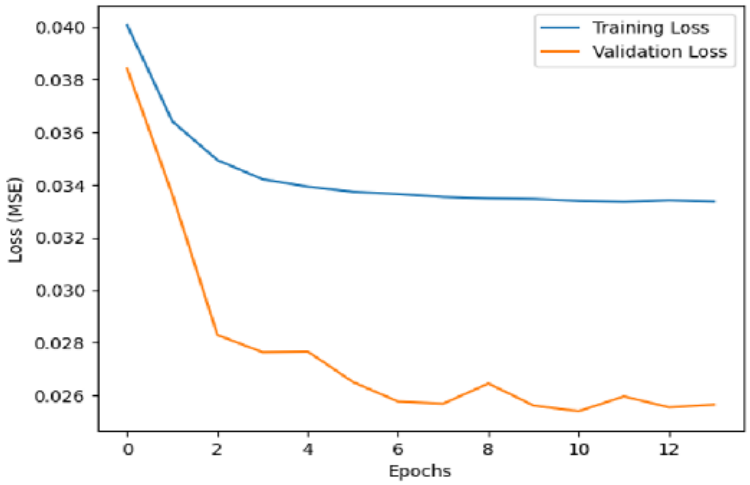

Figure 9: Autoencoder Training Curve for Motor Current and Temperature Signals

equipment failure.

Quantitative Metrics for the Autoencoder Fault Detection on Current-Temperature Signals

Table 2 summarises the diagnostic metrics for autoencoder-based fault analysis. To evaluate the model's performance in thermal analysis and optimisation of induction motors, several key metrics were employed using current and temperature datasets, including True Positive Rate (TPR), False Positive Rate (FPR), Precision, Recall, and F1-score. These indicators offer critical insights into the model's capacity to detect and classify anomalies responsible for overheating, thereby supporting predictive thermal management and improved operational control.

The autoencoder demonstrated strong thermal anomaly detection with a True Positive Rate of 94.5%, indicating effective identification of abnormal thermal deviations from baseline motor temperatures. The False Positive Rate, at 4.3%, reflects the model's precision in maintaining thermal integrity without incurring excessive false alarms,

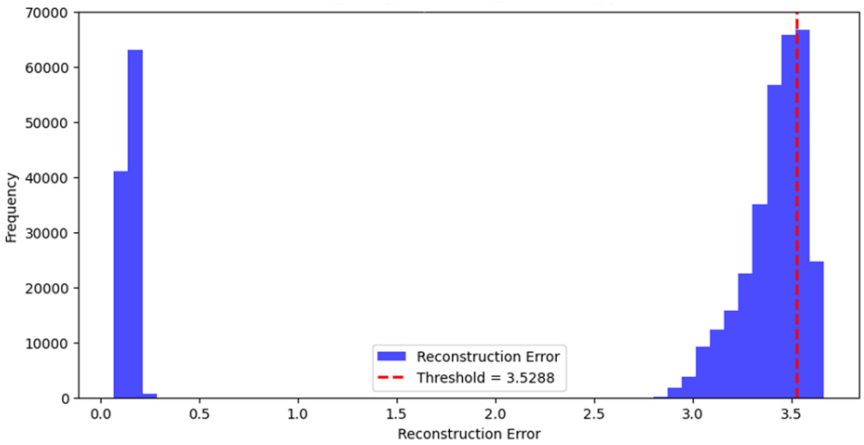

Figure 10: Error Distribution of Current-Temperature Signal Reconstructions at the 97th Percentile Threshold

thus minimising unnecessary interventions and optimising maintenance schedules. A Precision of 95.1% confirms the reliability of the model's classification of true thermal anomalies, ensuring confidence in its outputs for thermal control purposes. Matching the TPR, the Recall value of 94.5% demonstrates the model's sensitivity toward capturing nearly all thermal abnormalities. An F1-score of 94.8% signals a balanced and robust performance across thermal conditions, underscoring the model's suitability for consistent, non-intrusive thermal monitoring.

Each metric contributes to validating the model's real-time thermal optimisation capabilities: TPR and Recall quantify its effectiveness in detecting true thermal deviations, FPR prevents false alarms that could lead to inefficient maintenance, and Precision assures the dependability of issued alerts. The integrated F1-score encapsulates the overall stability and generalisation of model performance.

Overall, the autoencoder exhibits high efficacy across thermal domains, establishing itself as an effective tool for thermal analysis, fault detection, and operational optimisation in induction motor systems. This approach offers a non-intrusive and intelligent solution for early fault detection, thereby facilitating predictive maintenance and enhancing motor operational lifespan.

CONCLUSIONS

This study demonstrates that an autoencoder trained on synchronized current and temperature time series can detect thermal anomalies in induction motors with high sensitivity and precision. Training exclusively on normal operating data, and using reconstruction error as the anomaly indicator, the system effectively distinguished nominal and faulty states, achieving a True Positive Rate of 94.5% and an F1-score of 94.8%, while maintaining a low False Positive Rate of 4.3%. Rapid convergence of training and validation losses, along with stable validation performance, indicate strong generalisation on the experimental dataset. Exploratory analyses, including rolling averages, temperature trends, and correlation heatmaps, confirmed that phase currents and bearing housing temperatures contain complementary signatures of emerging thermal stress, validating their combined use for fault diagnosis.Practically, this approach offers a lightweight, data-driven solution for early fault detection and predictive maintenance, which can reduce unplanned downtime, lower maintenance costs, and improve energy efficiency in motor-driven systems. Future work should focus on validating this method on larger, more diverse datasets, enhancing model robustness through cross-validation and data augmentation, and exploring advanced architectures such as convolutional, recurrent, or variational autoencoders for richer temporal representation. Integration with real-time edge computing, multi-sensor fusion (including vibration and acoustic signals), and a structured cost-benefit analysis will further demonstrate operational value. Overall, the study establishes a practical foundation for scalable, AI-enabled thermal monitoring in industrial motor settings.

Table 2: Evaluation Metrics for the Autoencoder Fault Analysis with Current–Temperature Signals

Parameter	Current-Temperature Data (%)
True Positive Rate (TPR)	94.5
False Positive Rate (FPR)	4.3
Precision	95.1
Recall	94.5
F1-Score	94.8
Trained Epochs	12
Best Validation Loss	0.0256
Last Epoch Gradient	0.00035

Data Availability Statement

Data for this study are available at: https://data.mendeley.com/datasets/ztmf3m7h5x/6

REFERENCES

Abdulkareem, A., Anyim, T., Popoola, O., Abubakar, J., & Ayoade, A. (2025). *Prediction of Induction Motor Faults Using Machine Learning. Heliyon, 11*(1), 1-13. https://doi.org/10.1016/j.heliyon.2024.e41493

Aires, F. L., Galeno, G. D., Belchior, F. N., Oliveira, A. M., & Hunt, J. D. (2025). Enhancing Three-phase Induction Motor Reliability with Health Index and Artificial Intelligence-driven Predictive Maintenance. *Royal Society Open Science, 12*(5), 1-21. https://doi.org/10.1098/Rsos.241946

Al-Quraan, T. M., Vovk, O., Halko, S., Kvitka, S., Suprun, O., Miroshnyk, O., Nitsenko, V., Zayed, N. M., & Islam, K. A. (2022). Energy-saving Load Control of Induction Electric Motors for Drives of Working Machines to Reduce Thermal Wear. *Inventions, 7*(4), 2-19. https://doi.org/10.3390/inventions7040092

Azab, M. (2025). A Review of Recent Trends in High-efficiency Induction Motor Drives. *Vehicles, 7*(1), 1-50. https://doi.org/10.3390/vehicles7010015

Bahgat, B. H., Elhay, E. A., Sutikno, T., & Elkholy, M. M. (2024). Revolutionising Motor Maintenance: A Comprehensive Survey of State-Of-The-Art Fault Detection In Three-phase Induction Motors. *International Journal of Power Electronics and Drive Systems, 15*(3), 1968-1989. https://doi.org/10.11591/ijpeds.v15.i3.pp1968-1989

Berahmand, K., Daneshfar, F., Salehi, E. S., Li, Y., & Xu, Y. (2024). Autoencoders and Their Applications In Machine Learning: A Survey. *Artificial Intelligence Review, 57*(2), 1-52. https://doi.org/10.1007/s10462-023-10662-6

Bochkarev, I. V., Bryakin, I. V., Khramshin, V. R., Sandybaeva, A. R., & Litsin, K. V. (2021). Developing New Thermal Protection Method for AC Electric Motors. *Machines, 9*(3), 1-16. https://doi.org/10.3390/machines9030051

Elorza A. L., Almandoz, G., Egea, A., Ugalde, G., & Badiola, X. (2023). Study of Partial Discharge Inception Voltage in Inverter Fed Electric Motor Insulation Systems. *Applied Sciences (Switzerland), 13*(4), 1-38. https://doi.org/10.3390/app13042417

Habyarimana, M., & Adebiyi, A. A. (2025). A Review of Artificial Intelligence Applications in Predicting Faults in Electrical Machines. *Energies, 18*(7), 1-21. https://doi.org/10.3390/en18071616

Mhaske, P., Ghosh, S., Birajdar, R., & Gosavi, K. (2024). Effect of High Temperature On Electromagnetic Performance of Canned Induction Motor. In Proceedings of the 3rd International Conference for Innovation in Technology (pp. 1-6). https://doi.org/10.1109/INOCON60754.2024.10512206

Morikawa, K., & Katsura, S. (2022). Investigation into Increasing the Motor-drivable Current Using a Thermoelectric Cooling Module. *Power Electronics and Drives, 7*(1), 279-289. https://doi.org/10.2478/pead-2022-0021

Morikawa, K., & Katsura, S. (2023). Thermoelectric Cooling Application to Motors for High-power Operation. *IEEJ Journal of Industry Applications, 12*(2), 145-152. https://doi.org/10.1541/ieejjia.22004623

Paul, B., & Manohar, V. J. (2025). A Comprehensive Survey On Real Time Induction Motor Failure Diagnosis and Analysis. *ASEAN Engineering Journal, 15*(1), 199-206. https://doi.org/10.11113/aej.V15.22096

Polo, S., Rubio, E. M., Marín, M. M., & Sáenz de Pipaón, J. M. (2025). *Evolution and Latest Trends in Cooling and Lubrication Techniques for Sustainable Machining: A Systematic Review. Processes, 13*(2), 1-54. https://doi.org/10.3390/pr13020422

Reyes-Malanche, J. A., Villalobos-Pina, F. J., Ramırez-Velasco, E., Cabal-Yepez, E., Hernandez-Gomez, G., & Lopez-Ramirez, M. (2023). *Short-circuit Fault Diagnosis on Induction Motors through Electric Current Phasor Analysis and Fuzzy Logic. Energies, 16*(1), 1-15. https://doi.org/10.3390/en16010516

Soltani, M., Nuzzo, S., Barater, D., & Franceschini, G. (2022). *Investigation of the Temperature Effects on Copper Losses in Hairpin Windings. Machines, 10*(8), 1-13. https://doi.org/10.3390/machines10080715

Tabora, J. M., Correa. S. J. L., Ortiz, M. E., Mota, S. T., Arrifano, M. A. R., de-Lima, T. M. E., & Holanda, B. U. (2024). *Exploring the Effects of Voltage Variation and Load on the Electrical and Thermal Performance of Permanent-magnet Synchronous Motors. Energies, 17*(1), 1-16. https://doi.org/10.3390/en17010008

Tazerart, F., Kerrouche, F., Azib, A., & Rekioua, T. (2024). Improving Efficiency Through the Optimisation of Energy Losses In An Induction Machine for Electric Vehicle Propulsion. *Journal of Renewable Energies, 27*(1), 67-80. https://doi.org/10.54966/jreen.v27i1.1158

Tikadar, A., Joshi, Y., & Kumar, S. (2024). In-slot Cooling Enabled Heavy Rare-earth Free High Power Density Electric Motor for EV Application. In 2024 IEEE Transportation Electrification Conference and Expo (pp. 1-8). https://doi.org/10.1109/ITEC60657.2024.10599028.

Usman, A., & Saxena, A. (2025). Technical Roadmaps of Electric Motor Technology for Next Generation Electric Vehicles. *Machines, 13*(2), pp 1-27. https://doi.org/10.3390/machines13020156

Venugopal, G., Udayakumar, A. K., Balashanmugham, A., Houran, M. A., Alsaif, F., Elavarasan, R. M., Raju, K., & Alsharif, M. H. (2023). Fault Identification and Classification of Asynchronous Motor Drive Using Optimisation Approach with Improved Reliability. *Energies, 16*(6), pp. 1-25. https://doi.org/10.3390/en16062660

Yu, X., Chen, D., Wu, X., & Ai, M. (2024). The Influence of Loss Distribution on the Temperature Field of High-speed Induction Motor. *IEEE Access, 12*(2), 40196-40203. https://doi.org/0.1109/ACCESS.2024.3373544

Zeybek, Y., Kayış, C., & Diler, E. A. (2025). *Improving Electrical Conductivity of Commercially Pure Aluminium: The Synergistic Effect of AlB8 Master Alloy and Heat Treatment. Materials, 18*(2), 1-32. https://doi.org/10.3390/ma18020364

Zhang, Y., Zhang, Y., Pan, X., Zhao, B., He, J., Han, Y., Zhang, J., Wang, X., Yu, Z., Bu, G., & Ye, J. (2022). Equivalent Modeling Method of Induction Motor Contribution to Short-circuit Current. Energy Reports, 8(13), 1202-1210. https://doi.org/10.1016/j.egyr.2022.08.102

Zhao, X., Cui, H., Teng, Y., Chen, Z., & Liu, G. (2023). Design and Analysis of A High Loss Density Motor Cooling System with Water Cold Plates. Global Energy Interconnection, 6(3), 343-354. https://doi.org/10.1016/j.gloei.2023.06.008